Chapter 14
Evaporation in Arid Regions

Ichiro Tamagawa

Abstract Arid areas are among the typical ground types. In this chapter, evaporation in arid areas is introduced. Evaporated water vapor is carried by turbulence in the surface boundary layer, as is well described by the Monin–Obukhov similarity theory. A practical method of evaluating the evaporation amount from deserts is introduced here. Additionally, the dry surface layer in sandy soil is mentioned. Evaporation occurs under the soil surface, and the behavior of the evaporated water vapor in the dry surface layer connects the ground and the atmosphere.

Keywords DSL · HEIFE · Monin–Obukhov similarity · Sand desert · SBL · Turbulence

14.1 Introduction

This chapter introduces the basic idea for treating water and water vapor movement over or under the ground surface in arid areas, especially from the viewpoint of direct in situ observations.

The United Nations Environment Program (2006) said that the aridity index, which is the ratio of the precipitation amount to the potential evaporation amount, is one of the estimators commonly used to measure aridity. Aridity indices less than 0.20 mean that precipitation supplies under 20% of the water required for optimum plant growth. Areas with aridity indices less than 0.05 are classified as "hyperarid" and occupy 7.5% of the world. In contrast, areas with aridity indices from 0.05 to 0.20, occupying 12.1% of the world, are classified as "arid." The land covers in these areas are mostly sparse with no vegetation.

In this chapter, sand deserts are imaged as the simplest samples to describe the water movement through the ground surface, although there are other types of surfaces, such as oases, lakes, rivers, and other types of deserts. The water movement

I. Tamagawa (✉)
River Basin Research Center, Gifu University, Gifu, Japan
e-mail: tama@green.gifu-u.ac.jp

F. Li et al. (eds.), *River Basin Environment: Evaluation, Management and Conservation*, https://doi.org/10.1007/978-981-19-4070-5_14

from rivers or lakes to deserts and its consumption by evaporation are of great interest and importance to the understanding of the water budget of an area. However, this chapter focuses on one-point scale processes as basic components of water movement. As frequently done, we considered them one-dimensionally, which implies a horizontally homogeneous surface and that water and water vapor move only vertically. These processes seem simple because only evaporation occurs on the sand surface (i.e., without vegetation activity). Thus, simple physical processes are expected to describe these phenomena.

14.2 Water and Water Vapor Movement over the Ground Surface and the Boundary Layer

Generally speaking, water vapor evaporating from the surface is carried by atmospheric motion, forms clouds, and falls as precipitation. In this chapter, we focused on the processes near the surface.

The air at the bottom of the atmosphere touches the ground surface and is heated by solar radiation during daytime and cooled by radiative cooling. Usually, air parcels (i.e., small volumes of air) can move in limited layers and cannot move into the upper atmosphere because the potential temperature of the upper atmosphere is higher than that of the lower atmosphere. Potential temperature is defined as the temperature of the air compressed adiabatically to the reference pressure 1000 hPa, where the state with no heat exchange is called the adiabatic state. It is useful in considering the vertical movement of air because the air temperature varies by expansion or compression because of pressure. The difference in the potential temperature between an air parcel and the surrounding atmosphere determines the buoyancy force acting on the parcel. Only nonadiabatic processes, such as condensation heating, heat exchange on the ground surface, and radiative heating/cooling, can change the potential temperature. Thus, meteorologists prefer using the potential temperature in comparing the air at different altitudes.

The air parcel heated on the ground surface has a higher potential temperature and thus obtains an upward buoyancy force. However, the upward movement of the air parcel eventually stops, and it stays inside a shallow layer because the upper atmosphere has a higher potential temperature. The heated air is then mixed into the layer. Even at nighttime, the lower part of the mixed layer is cooled on the cooled surface, but the air over the cooled layer remains mixed because the cooled air layer does not grow well because of the negative buoyancy force.

The shallow layer where the air affected by surface conditions mostly stays is called the atmospheric boundary layer (ABL). Its depth is typically about 1 km, which varies because of climate and weather conditions. The water vapor coming into the atmosphere from the ground surface is well mixed in the ABL at daytime but does not spread well and stays in cool shallower layers at nighttime. We call the daytime ABL the mixing layer, where the water vapor concentrations become

uniform, except that for the surface layer. The surface layer is the lowest part of the ABL, where the short distance from the ground surface limits turbulent mixing. This lowest layer is called the surface boundary layer (SBL), typically the lowest 10% of the ABL. At nighttime, the atmosphere is cooled mainly by the radiatively cooled ground surface. The potential temperature decreases from the bottom. This stabilizes the layers near the ground surface (i.e., the vertical motion of air is reduced). If evaporation occurs, the evaporated water vapor stays in the lowest part of the ABL on the surface (almost the SBL), and its concentration increases at lower heights. These processes are explained in many textbooks of meteorology (e.g., Chap. 4 of Fleagle and Businger 1980; Chap. 1 of Stull 1988).

In summary, water vapor is produced by evaporation at the bottom of the atmosphere (i.e., the ground surface) and expands in the ABL. The SBL has a big role in bringing water vapor from the surface to the atmosphere. Additionally, we may ask about how water vapor can move into the atmosphere over the ABL. On the upper boundary of the ABL, turbulent mixing brings water vapor into the upper atmosphere through entrainment, but the amount of mixing is relatively much smaller than that in the SBL. Convective clouds, such as cumulonimbus, bring much water vapor through the convective air motion, which is driven by the heat released through condensation. In such a case, the ABL becomes a substructure under the cloud. In this chapter, we discuss an atmosphere without strong cloud activity to neglect such process. This is consistent with our topic on arid areas.

14.2.1 Surface Heat Budget and Turbulent Transport of Water Vapor

Evaporation consumes energy. Energy is another limiting condition of evaporation besides water existence itself. From the energy conservation law, the surface energy budget (14.1) shows the limiting condition for evaporation. The equation is written for the energy emitted from or absorbed by a unit area of the surface for a unit of time, and it shows the energy conservation law. Each term is called the vertical component of heat flux, frequently abbreviated as "heat flux." Its unit is W m^{-2} in the S.I. unit system. Because we considered only vertical components, the equation can avoid complicated vector mathematics. The equation can be written as

$$(1-\alpha)Q_s + Q_{ld} - Q_{lu} = H + \lambda E + G, \quad (14.1)$$

where Q_s is the shortwave (solar radiation) flux on the surface, α is the surface albedo, which is the reflectivity of the shortwave radiation, Q_{ld} is the downward longwave radiation flux from the atmosphere to the surface, Q_{lu} is the longwave radiation emitted from the ground surface to the atmosphere, H is the heat transported from the surface to the atmosphere, called the sensible heat flux, λE is the latent heat consumed by evaporation E at the ground surface, called the latent

heat flux, and G is the heat flux going into the ground. The sign of each term follows its explanation, and the terms can be negative to indicate the opposite direction. The left side of the equation shows radiative fluxes into the surface, and the right side shows fluxes from the surface. The equation is correct when water evaporates from the surface, when other chemical reactions or physical processes relating to energy do not occur, and the surface is just plain without depth. However, for surfaces with vegetation, the energy heating or cooling vegetation must be considered. In such cases, the canopy layer with some height is considered instead of an ideal surface without depth. However, such treatment was skipped here for simplicity. Still, including the heat budget of the ground with heat capacity variation due to the soil water content is important. The heat brought by precipitation must also be considered to close the heat budget correctly. As for arid surfaces, evaporation and heat consumption may occur under the surface. This point will be mentioned in a later section. Here we treat evaporation as occurring at the surface.

The sensible heat flux H and latent heat flux λE are carried by atmospheric processes. Heat and water vapor transported by molecular diffusion processes may dominate just on the surface; molecular diffusion loses its dominance only in the millimeter scale, where turbulent transfer processes dominate in other layers.

Air motion is turbulent in almost all the atmosphere. A textbook on fluid dynamics said that the Reynolds number $R_e = Uz/\nu$ indicates whether a flow is laminate or turbulent, where U is the speed of the air motion, z is the height used as the typical length scale of the air motion, and ν is the dynamic viscosity coefficient of the air. For example, a 1- m s^{-1} wind speed at a 1- m height above the ground surface and at 300 K ($\nu = 15.8 \times 10^{-6}$ $m^2 s^{-1}$) has a Reynolds value of more than 6×10^4, which is high enough to indicate turbulent motion.

Under turbulent conditions, wind and other atmospheric variables show much fluctuation in time and space. Horizontal homogeneity should be redefined to show the horizontal homogeneity of the turbulence statistics. Under turbulent conditions, heat, water vapor, and momentum are transferred by turbulence. The effects of molecular diffusion can be neglected from the viewpoint of transferring processes but not for the dissipation processes of turbulent motion. This is because turbulent motion progresses from large to small scales and dissipates its fluctuation in very small scales because of molecular diffusion and viscosity.

The turbulent fluxes H and λE can be measured using the vertical wind speed, temperature, and humidity. Only the vertical components of wind are important because we assumed horizontally homogeneous conditions and that the horizontal movement of heat and water vapor has no effect on the surface-to-atmosphere transport. Turbulent transfer processes can be measured using sensors in the field. The measurement must cover the turbulent fluctuation of water vapor, wind, and so on. Usually, sonic anemometer thermometers (SATs) and infrared gas analyzers are used. These instruments can measure at a sampling rate of greater than 10 Hz. The gas analyzer can measure the water vapor density and, often, the CO_2 density. Thus, it is frequently used to observe CO_2 absorption rates such as that over forests. The results of such carbon-related studies may be shown in some other chapters.

Back to the description of H and λE, the turbulent transport of H and λE can be evaluated using (14.2) and (14.3) in a technique called the eddy covariance method:

$$H = \rho\, C_{\mathrm{p}}\, \overline{w'T'}, \tag{14.2}$$

$$\lambda E = \lambda\, \rho\, \overline{w'q'}, \tag{14.3}$$

where ρ is the density of air, C_{p} is the specific heat of a unit mass of air at constant pressure, w is the vertical component of wind velocity, T is the absolute temperature, and q is the specific humidity, which is the water vapor mass per unit mass of air. The symbols $\bar{}$ and $'$ show the average and turbulent fluctuation components of each variable. For the temperature turbulent fluctuation, $T' = T - \bar{T}$, $q' = q - \bar{q}$, and $w' = w - \bar{w}$. The averaging period and sampling rate should be considered the statistics of turbulence such as those written in terms of the cospectral density function in Kaimal and Finnigan (1994). Roughly saying, 30-min recording with 10-Hz sampling is a typical configuration for observations on the point from a height of several tens of meters.

The meaning of the covariance $\overline{w'q'}$ can be explained as follows: the amount of water vapor transported vertically by wind for a unit horizontal area for a unit time can be expressed as $\rho_{\mathrm{v}} w$, where ρ_{v} is the density of water vapor, considering that w multiplied by a short time is the volume passing the unit area for this short time and that the density multiplied by the volume gives the mass. So, on average, $E = \overline{\rho_{\mathrm{v}} w} = \overline{\rho q w}$. The air density can be usually treated as a constant. Here, we used ρ to represent the constant air density, including water vapor itself. In this case $\rho_{\mathrm{v}} = \rho q$. When w, q are divided into mean components $\bar{w}, \bar{q}$ and turbulent components $w'q'$, given $\overline{w'} = 0$ and $\overline{q'} = 0$, the average water vapor flux (i.e., evaporation) can be shown as

$$E = \rho\, (\bar{w}\, \bar{q} + \overline{w'q'}). \tag{14.4}$$

The mass conservation law gives

$$\frac{\partial \rho}{\partial t} = -\left(\frac{\partial (\rho u)}{\partial x} + \frac{\partial (\rho v)}{\partial y} + \frac{\partial (\rho w)}{\partial z} \right), \tag{14.5}$$

where x, y represent the horizontal coordinates and u, v are the horizontal components of wind. (14.5) can be read as the convergence of mass flux resulting in increased mass. Then, we assumed horizontally homogenous conditions with constant ρ. (14.5) thus becomes $\frac{\partial \bar{w}}{\partial z} = 0$ because $\frac{\partial \rho}{\partial t} = \frac{\partial (\rho u)}{\partial x} = \frac{\partial (\rho v)}{\partial y} = 0$. On the surface, $\bar{w} = 0$ leads to $\bar{w} = 0$ everywhere. Therefore,

$$E = \rho\, \overline{w'q'}. \tag{14.6}$$

In the same way, $H = \rho\, C_\mathrm{p}\, \overline{w'T'}$, considering that the heat consumed for the temperature change in open conditions can be expressed using C_p. The heat passed to or removed from the air on the surface gives the temperature fluctuation $C_\mathrm{p}T'$ because the heating process occurs at constant pressure conditions. H can be so as in (14.2).

The temperature T is not conserved in vertical motions, as mentioned earlier. Thus, the potential temperature must be used in considering atmospheric motion. Here, we assumed that the turbulence measurement is done at a fixed position not so far from the surface. The atmospheric pressure at some height is determined by the gravitational force acting on the air column above the height because vertical air motion usually has small acceleration to keep the balance between the pressure gradient force and gravity. This pressure is called hydrostatic pressure. The pressure changes only gradually because it is caused by the vertically integrated gravity force for all air above the point. Therefore, the pressure on the surface can be thought of as constant in a short time (e.g., 30 min). The pressure difference between the surface and the measurement height can be thought of as very small. Thus, the measured T' can be used as the surface value. In very strict discussions, small temperature corrections due to the pressure difference between the measuring height and surface might be needed, but these are usually negligible. Only the heat used at constant pressure conditions, which includes the work done by the density change due to temperature change, is considered to obtain the heat flux in (14.2).

In actual conditions, we must consider a bit more factors than those from the simple ideal conditions used in the above discussions. For instance, the ground surface may not be perfectly horizontally flat and may have some slopes and undulations. The direction of the heat flux must also be reconsidered. We can assume average wind flows along the surface, and we can use the direction perpendicular to the surface instead of the geometrically vertical direction because such coordinate change can keep the assumed horizontally homogenous surface. The assumption used over the horizontally homogenous surface means $\left|\frac{\partial s}{\partial x}\right|, \left|\frac{\partial s}{\partial y}\right| \ll \left|\frac{\partial s}{\partial z}\right|$ for some variable s to disregard its horizontal difference. Especially for wind, the important vertical component of the wind velocity obeys $\frac{\partial \bar{w}}{\partial z} = 0$, and $\bar{w} = 0$ at the surface gives $\bar{w} = 0$ everywhere. No mean vertical wind condition is important because the fluxes caused by the mean wind often show very large heat and water vapor transport. Moreover, if a geometrical $\bar{w}$ exist, the mean transport seems to be canceled over other places because the amount of air mass between the observation height and the surface is expected to be conserved. Vertically, we may expect the turbulent transfer to be more representative than the mean transfer. The turbulence statistical values along to the direction with the largest gradient of some variables are expected to be more representative, and the gradient perpendicular to the surface is the largest over the generally sloped and undulated surface.

For a more detailed calculation, we may have to consider the average of the vertical mass flux by turbulence. Warm air tends to move upward and cold air downward over a heated surface at daytime, resulting in a downward mass transfer by turbulence because lower-density air is exchanged with higher-density air and

vice versa at nighttime. These phenomena result in compensating flow through a very small mean motion of air, which may be smaller than the sensor's resolution and preciseness. Quantifying the water vapor produced by evaporation may be necessary to give the mean vertical transfer of heat aside from vapor transfer. If we have a perfectly flat uniform observation place with a perfectly precise sensor, transport can be detected as a vertical motion. However, the resolution and preciseness of the sensors and the flatness or homogeneity are not enough. Thus, we must consider these points in what is called the Webb, Pearman, and Leuning correction (Webb et al. 1980; Leuning 2007). This correction is sometimes important in evaluating CO_2 flux, but we do not want to dwell on this point here. For details, the readers are referred to Chap. 4 of Foken (2008).

14.2.2 Monin–Obukhov Similarity Describing Turbulence Statistics

The turbulent fluxes and other statistics relating to turbulence can be connected to each other, including the mean field by the Monin–Obukhov similarity (Chap. 5 of Stull 1988). The theory was developed in the 1940s and validated using turbulent observation experiments from the 1960s. Only a brief introduction is included here to discuss arid conditions.

The target is a horizontally homogenous and steady condition in the SBL with a roughly 100-m depth. Each turbulent flux becomes constant because the horizontally homogenous and steady condition gives no vertical divergence or convergence. In this condition where no other variations exist, the most important values in determining the vertical profile of the average values are the turbulent fluxes. In the simplest case when the buoyancy force does not work because of the constant potential temperature, only the Reynolds stress transfers horizontal momentum in the vertical direction through $\overline{u'w'}$. The vertical gradient of the averaged wind is $\partial\bar{u}/\partial z$, where $\bar{u}$ shows the mean wind component along the averaged wind direction, which is horizontal over the horizontally uniform surface, and z, w are the vertical coordinate and component of wind, respectively. The turbulent fluctuation of wind mixes the air parcel originally moving with other air on average. This means that larger $\bar{u}$ values at high altitudes give positive u' to the smaller $\bar{u}$ values at low altitudes because of the downward vertical motion with negative w' and vice versa. The covariance $\overline{u'w'}$ is always statistically negative over horizontally homogeneous and steady conditions. The drag velocity u_* is defined as $u_*^2 = -\overline{u'w'}$ to show the scale of the turbulent fluctuation. Considering the dimensions of each variable, $\frac{z}{u_*}\frac{\partial\bar{u}}{\partial z}$ can be a nondimensional variable. Thus, if there is no other variable, it should be constant.

$$\frac{kz}{u_*}\frac{\partial \bar{u}}{\partial z} = 1, \tag{14.7}$$

where the constant k is called the *von Kármán* constant, whose value is found to be almost 0.4. This kind of discussion is called "dimensional analysis" and gives a useful framework for complicated phenomena, and discussions on turbulence frequently use it. The essential point of dimensional analysis is in the selection of variables based on physical images. This relationship can also be modeled using simple physical models such as $|u'| \sim |w'| \sim l\frac{\partial \bar{u}}{\partial z}$, where l shows the length scale of the turbulent motion by considering the Taylor expansion of $\bar{u}$ as a function of z. The air parcel with different mean wind speeds at different heights gives a wind speed fluctuation $l\frac{\partial \bar{u}}{\partial z}$, and the turbulent wind is well mixed to forget the direction $|u'| \sim |w'|$. One more assumption is that the turbulent length scale is proportional to the height, $l = kz$. Then, $u_*^2 = -u'\bar{w}' = -\left\{kz\left|\frac{\partial \bar{u}}{\partial z}\right|\right\}^2$ can be written as (14.7), with k as the coefficient of the turbulent length scale, which is the eddy size including the information of the correlation coefficient for the momentum flux. The covariance $u'\bar{w}'$ becomes negative because the upward moving ($w' > 0$) air parcel has a lower mean wind speed ($u' < 0$), as mentioned earlier. Integrating (14.7) from $z = z_0$ to z, the average wind speed $\bar{u}$ as the function of height z,

$$\bar{u} = \frac{u_*}{k}\log\left(\frac{z}{z_0}\right), \tag{14.8}$$

is obtained, where z_0 is the imaginary lower limit of the turbulent layer to have $u = 0$. z_0 is called the roughness height, and it shows the surface roughness for drag efficiency. It is worth mentioning that hydraulics uses a little bit different definition. Thus, we must be careful in using roughness values from hydraulics.

The relationship shown in (14.8) is called the logarithmic law, which is frequently observed in the near-wall region of many fluids without buoyancy force. The height z is not necessarily the geometrical height from the surface. Often, $z - d$ is used to show the appropriate turbulent eddy size using the zero plane displacement d, and the definition of z itself may be ambiguous over very rough surfaces. The values of z_0 and d are frequently connected to the representative height of the obstacle over surfaces like a building height or a forest height. Here, we considered a flat surface to ignore such point, but sand dunes usually exist on real sand deserts. We skipped these details and focused on a flat surface.

The thermal stratification of the atmosphere gives another buoyancy force effect. Thus, the turbulent status must be considered with buoyancy force caused by temperature fluctuations. Temperature turbulence must have a strong relation to the sensible heat flux at the surface with the coefficient $\frac{g}{T}$, which connects the temperature fluctuation with the buoyancy acceleration, where g is the gravitational acceleration. The Monin–Obukhov stability

$$\frac{z}{L} = \frac{kzgT_*}{\bar{T}\,u_*^2}, \tag{14.9}$$

is a nondimensional parameter showing the effect of buoyancy on turbulence. T_* is the scale parameter of the temperature fluctuation defined as $u_*\,T_* = -\overline{w'T'}$ using u_*. By the same kind of turbulent transfer expression as u_*, $L = \frac{\bar{T}\,u_*^2}{kgT_*}$ is called the Obukhov length. The physical meaning of the Obukhov stability can be considered using the kinematic energy equation of turbulence motion in a horizontally uniform and steady condition. z/L corresponds to the ratio of the buoyancy decay (negative production) rate and the shear production rate of turbulent kinematic energy in the form of a scaling parameter. For details, please see Stull (1988). The sign of z/L is determined by T_*, in other words, by $-\overline{w'T'}$. A positive z/L shows that the turbulent kinetic energy produced by wind shear is decreased by the negative buoyancy force suppressing the turbulence under "stable" conditions. In contrast, a negative z/L shows that the turbulent energy additionally produced by buoyancy force enhances turbulence under "unstable" conditions. z/L equal to zero means no buoyance force under "neutral" conditions, which are the same as the logarithmic law condition. Strictly speaking, the virtual temperature should be used instead of T and the one used for T_* to include the effects of humidity on air density, but we did not use it here for simplicity and as it has little effect in arid conditions.

(14.7) can be expanded by incorporating it with z/L:

$$\frac{kz}{u_*}\frac{\partial \bar{u}}{\partial z} = \phi_m\left(\frac{z}{L}\right). \tag{14.10}$$

ϕ_m shows some experimental function of z/L, which is expected to be universal to all measurements satisfying the used assumption. The temperatures $T, \bar{T}$, and T_* are used instead of the potential temperature variables. This has been widely accepted in the literature because the potential temperature $\theta = T\left(\frac{P_0}{P}\right)^{\frac{C_p}{R}}$, where P, P_0 are the air pressure at the point and that at reference, respectively, and R is a gas constant for a unit mass of air, which has a factor determined only by pressure and is treated as a constant value. Thus, the $\frac{\theta'}{\theta} = \frac{T'}{T}$ relationship exists in the equations used above. For the vertical gradient, we must consider the difference between θ and T because θ is conserved in adiabatic motion, where turbulence is included, whereas T is not. By using the dry adiabatic lapse rate Γ_d,

$$\frac{\partial \bar{\theta}}{\partial z} = \left(\frac{P_0}{P}\right)^{\frac{C_p}{R}}\left(\frac{\partial T}{\partial z} + \Gamma_d\right), \tag{14.11}$$

where $\Gamma_d = \frac{g}{C_p} \sim 0.01\ \mathrm{K/m}$, which is small enough to neglect. In this case, the temperature profile is written as.

$$\frac{kz}{T_*}\frac{\partial \bar{T}}{\partial z} = \phi_h\left(\frac{z}{L}\right), \tag{14.12}$$

where ϕ_h is the empirical function of z/L for temperature, which is thought to be same for other scalar variables such as the specific humidity of water vapor and CO_2 concentration. For specific humidity,

$$\frac{kz}{q_*}\frac{\partial \bar{q}}{\partial z} = \phi_h\left(\frac{z}{L}\right), \tag{14.13}$$

where q_* is defined as $\overline{w'q'} = -u_*q_*$.

The integration of (14.10), (14.12), and (14.13) between appropriate heights, sensible heat flux, and latent heat flux may be written as

$$H = \rho C_p(-u_*T_*) = \rho C_p C_h U(T_s - T_a), \tag{14.14}$$

$$\lambda E = \rho\lambda(-u_*q_*) = \rho\lambda C_e U(q_1 - q_a), \tag{14.15}$$

where C_h, C_e are the so-called bulk coefficients for heat and water vapor, respectively. These coefficients are not only functions of z/L but also parameters expressing surface conditions such as roughness height and integration range. In this chapter, (14.10) is integrated from the roughness height to the observation height, (14.12) is done from the surface to the observation height, and (14.13) is from some lower height to the observation height. The Monin–Obukhov similarity theory is for turbulence statistics; however, the region very near the surface is out of the applicable region, and some other relationships, including molecular diffusion, may be assumed applicable to determine the relationship between the surface temperature and the air temperature. The integration itself can be done with some accuracy, and (14.14) may be expected.

The bulk equation of heat fluxes is used in numerical models such as weather prediction models because of its lower boundary condition with the surface heat budget equation. Even if we measure the turbulent flux directly, the comparison between the measured turbulence statistical values and the mean values can indicate the representativeness of the measurement by considering the assumptions used in the model to connect them.

Turbulence statistics other than fluxes can also be applied using the Monin–Obukhov similarity. For example, the standard deviation of the turbulent fluctuation of the vertical component of wind σ_w and temperature σ_T can be expressed as functions of z/L after normalization using u_* and T_*:

$$\frac{\sigma_W}{u_*} = \phi_w\left(\frac{z}{L}\right), \tag{14.16}$$

$$\frac{\sigma_T}{T_*} = \phi_T\left(\frac{z}{L}\right), \tag{14.17}$$

where ϕ_w and ϕ_T represent some function.

14.2.3 Surface Heat Budget and Turbulent Transportation of Water Vapor in Arid Areas

In arid areas, the fundamental physics is same, but the assumptions used in the above discussion might not be so. Thus, observed data are needed to elucidate these problems. The results of the Heihe River Basin Field Experiment (HEIFE; 1989–1993) (Mitsuta 2005) are introduced as examples. Intensive observations were made over a sand desert in northwest China in 1991 and 1992 for an early project measuring turbulent fluxes for a long-time evaluation of heat and water budgets. The Kaijo DAT-300 used as the SAT for the project was an already matured one, and the infrared gas analyzer for water vapor Kaijo AH-300 was in the development stage as an open-path gas analyzer of water vapor for field observations. A stable gas analyzer for water vapor and carbon dioxide started to be used for observations about after 2000. The data recording system had abilities inferior to those of current systems, especially as regards storing capacity. For these reasons, we could not continuously observe turbulent fluxes in those days but could observe mean meteorological variables. We had to connect the mean observation results with the turbulent flux measurement results at that time. Now, we can use continuous turbulent observations with solar panels and tough data loggers with Internet connection in our laboratory. However, considering the relationships among many statistics is still largely unexplored.

As for the turbulence statistics, (14.17) and the same relationship for q are examined:

$$\frac{\sigma_q}{|q_*|} = \phi_q\left(\frac{z}{L}\right). \tag{14.18}$$

The denominator in the left figure must be an absolute value because the signs of q_* and T_*, which correspond to the sign of z/L, are independent. Figure 14.1 shows the relationships between T and q for unstable conditions. ϕ_T and ϕ_q are expected to be the same because they are passively transferred by wind. ϕ_T in Fig. 14.1 shows a very large scatter in the range of $-\frac{z}{L} < 0.1$. This is because the temperature fluctuation and sensible heat flux must reach zero in neutral conditions. If the turbulent fluctuation of temperature were driven only by the movement of the air parcel due to turbulent motion as assumed by the Monin–Obukhov similarity, the temperature fluctuation and vertical transport of heat would vanish at all. This means that the value of ϕ_T is undefined in neutral conditions, which means $\frac{z}{L} = 0$. Usually, we have some temperature fluctuations caused by horizontal inhomogeneity or other

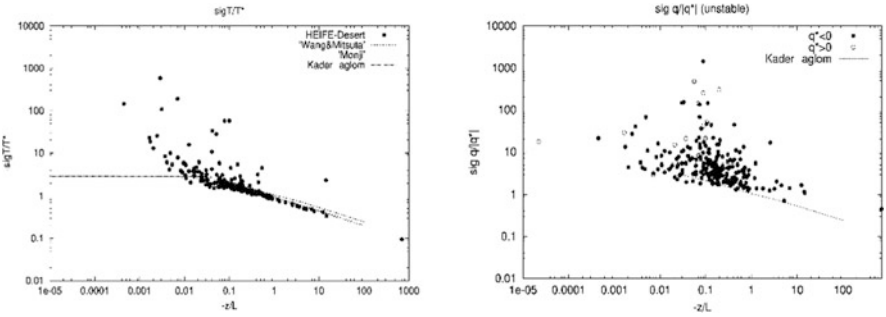

Fig. 14.1 The nondimensional standard deviation of the turbulent fluctuation of temperature and specific humidity. "sigT" and "sig q" are σ_T and σ_q in (14.17) and (14.18), respectively. Wang and Mitsuta (1991), Monji (1973), and Kader and Yaglom (1990) showed such relationship in previously published papers but only for temperature. Even in right figure, because of the unavailability of turbulence data of water vapor from the literature, the same relationship as that of temperature was expected. These figures were reproduced from Tamagawa (1996)

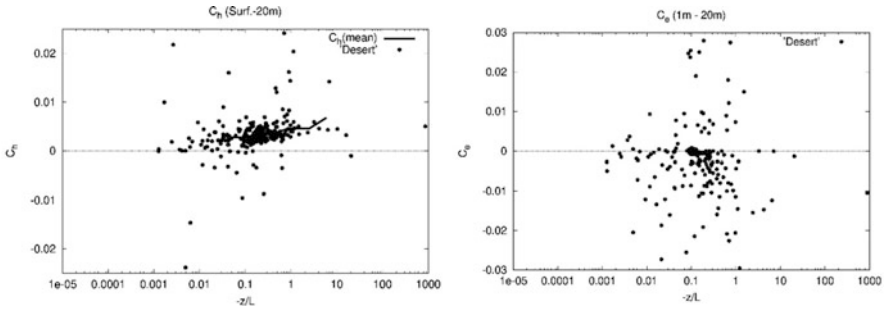

Fig. 14.2 The bulk coefficients calculated using observations (14.14) and (14.15). Data were taken from a desert station of the HEIFE project (1989–1993). The block averaged values are represented by thick lines in the Ch figure (after Tamagawa 1996)

phenomena, even in neutral conditions. Such fluctuations do not contribute to the vertical turbulent flux for T_* but contribute to σ_T, producing large σ_T/T_*. In unstable and stable conditions, temperature fluctuations caused by vertical motions and gradients become dominant, as supposed by the Monin–Obukhov similarity theory. As for ϕ_q in Fig. 14.2, the points show very large scatters. Only the lower edge of the distribution of points shows the same tendency as that seen in the temperature figure. This feature can be understood in the same way as that in the near-neutral condition and ϕ_T. The evaporation $\rho\, \overline{w'q'}$ from the arid surface is small due to the lack of moisture to give turbulent fluctuation and the vertical gradient of specific humidity. These contribute to the vertical transfer of water vapor, giving the q_* value, and some fluctuation caused by inhomogeneity or other factors gives σ_q to produce large ϕ_q. Only when the vertical transport of water vapor prevails can ϕ_q show the same behavior as that of ϕ_T outside of near-neutral conditions. The turbulent fluctuation of

water vapor may be considered the same as that of temperature with strong contamination of other fluctuations not related to the vertical transport of water vapor.

The first step in evaluating the amount of evaporation is connecting turbulent fluxes with the mean observation data. Figure 14.2 shows examples of the evaluation of the bulk coefficients for sensible heat and latent heat fluxes. The fluxes measured by the turbulent observation were compared with the mean temperature, specific humidity, and wind speed using (14.14) and (14.15). The observations of U, T_a, q_a were on the top of the observation tower (20 m), and the height of q_1 is the lowest point of the tower (1 m). The data were not screened so we could use all observed data to evaluate fluxes, although we selected data to very carefully evaluate, for example, the amount of carbon absorbed by a forest. Figure 14.2 shows only unstable conditions as examples. For the sensible heat and temperature, the bulk coefficient C_h shows some related, densely distributed points, although several data points show large scattering. C_h could be determined experimentally. The effect of the sand dune topography was included in the C_h behavior. In any way, the averaged C_h could be obtained. However, the data points scatter in a wide area for C_e, and even its negative values were frequently seen. This could be understood as follows: the small amount of evaporation from the dry sand surface gave a small q_*, $\partial q/\partial z$, giving unstable C_e, as recognized by looking (14.13). Also, the accuracy and resolution of the mean humidity might be doubtful. The directly measured turbulent water vapor flux E had reasonable results, showing water budget analysis in several weeks of evaporation in Mitsuta et al. (1995). The heat budget analysis that used (14.1) was done using the observed values in Mitsuta et al. (1995). The heat budget is almost close with a 10-day averaging with small residuals under 10 Wm^{-2}. The error of the daily heat budget was suggested to be caused by the heat flux into the ground G. We evaluated the very large variations in the soil temperature in very shallow depths caused by strong heating and cooling on the surface. Additionally, the temperature variation in deeper soil layers must be quantified. The annual cycle of deep soil temperature variations was evaluated using a thermal diffusion equation under the deepest observation temperature. The soil thermal characteristics were measured using sampled sand in a laboratory.

In the heat budget of (14.1), the radiation fluxes were measured using a pyranometer and a pyrgeometer for both directions. H could be evaluated from the mean temperature and the wind speed, and G could be determined using ground thermometers with special consideration for annual-scale long-time temperature variations. The remaining term LE could be evaluated as a residual of (14.1). Then, the evaporation rate E could be evaluated. Figure 14.3 shows the observed precipitation after 10-day averages with precipitation amount. Evaporation was stimulated by precipitation. The annual average of evaporation was about 120 mm/year, and that of precipitation was about 100 mm/year. The precipitated water was evaporated, and just a little more evaporation occurred to consume groundwater. The observed region is not so far from oases, and river water was used for irrigation. As the river “Heihe” flows into the desert to disappear with an endorheic lake of the Juyan Lake, the evaluated results seem reasonable.

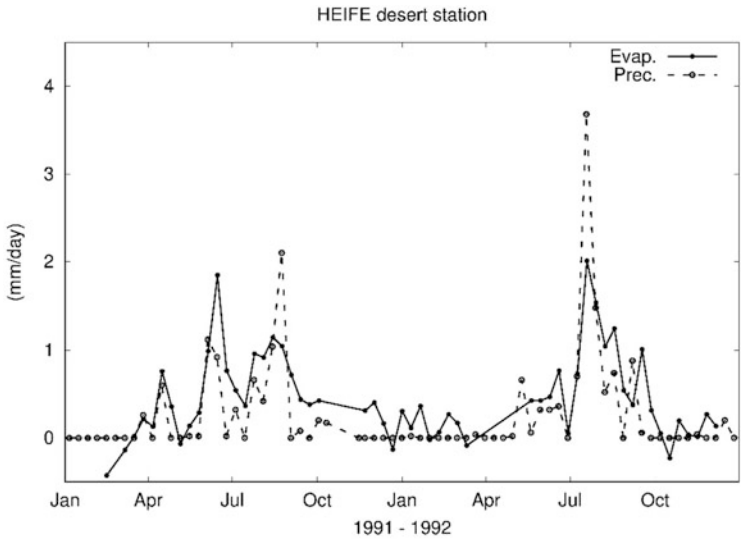

Fig. 14.3 The evaluated evaporation rate and observed precipitation at a desert station of HEIFE in 10-day averages (after Mitsuta et al. 1995)

Heat budget and analysis using turbulence were introduced to show an evaluation sample of evaporation in arid areas. The observation itself was of course tough, and careful analyses based on the knowledge of meteorology were required even in the simple surface condition of sand desert.

14.3 Water and Water Vapor Movement in Soil

One more short section is added to introduce the water movement in sands. Water movement in porous media is generally described by Darcy's law. The gradient of the water potential gives force for water to move against the resistant drag force caused by the flow with hydraulic conductivity. However, if large spaces (i.e., macropores) exist in soil, the water flow becomes turbulent, breaking Darcy's assumptions (Hillel 2004). The ground soil in humid areas has a crumb structure with macropores relating to vegetation activity, and vegetation has transpiration activities. Water movement in humid areas may be more difficult, but the soil in the sand desert is rather simple. The sand and the soil in the desert are well mixed by the wind, making them uniform without macropores or vegetation. Instead, of this simplicity, the soil pores are not filled with water, and the unsaturated layer of the soil must be considered. Even in humid areas, unsaturated zones may exist just on the surface, which we usually do not consider because they are shallow and because other points are more important. In arid areas, the unsaturated layer is developed much. For unsaturated soil, Philip and de Vries (1957) and de Vries (1958) gave a

framework for treating water and water vapor movement with temperature variations in soil using a set of equations. The full equations are skipped here to avoid too many equations and variables. They demonstrated the movement of liquid water due to its potential gradient and the water vapor movement due to the water vapor density gradient in unsaturated layers. The surface heat budget of (14.1) appears for temperature in the water movement analysis. In arid conditions, such as in sand deserts, the so-called dry surface layer (DSL) forms in the uppermost region of the soil. In DSL, liquid water does not move because the water in pores does not continue but is adsorbed on soil particles. Water vapor evaporates at deeper layers and diffuses in pores through the DSL to the sand surface and goes out to the atmosphere. Some brief details are shown below. The water vapor density in pores ρ_v, in the equilibrium state with the water in pores, is expressed as

$$\rho_v = \rho_0 e^{-\frac{\Psi g}{R_v T}}, \tag{14.19}$$

where R_v shows the gas constant for a unit mass of water vapor, and ρ_0 shows the saturated water vapor density at temperature T over the plain water surface. Ψ is expressed in units of height, following common usage in soil physics. Ψg shows the potential, that is, the energy for unit mass, of liquid water differing from the plain surface state due to capillary and adsorption by sand. The value of Ψ decreases rapidly as the soil water content decreases.

(14.19) is called Kelvin's equation. ρ_0 is a function of T, and the exponent of e also includes the temperature T. From both effects, ρ_v is determined by T and Ψ. The factor $e^{-\frac{\Psi g}{R_v T}}$ very rapidly decreased as the soil water content decreased. In the DSL, the profile of ρ_v becomes a quasi-steady state because changes ρ_v is connected to soil water content through Ψ and soil water works as the source or sink of water vapor. The water vapor flux becomes constant in the DSL to keep a steady ρ_v. This short consideration gives a picture of DSL: evaporation occurs at the bottom of DSL, which is called the drying front, and the produced water vapor is transported to the surface. The direct evaporation from the sand surface is negligible. ρ_v at the surface is approximately the same as that of the atmosphere because in arid conditions, the gradient of specific humidity q is small because of the small evaporation in SBL, as shown in (14.13). The evaporation rate E can be expressed as

$$E = K \frac{\rho_v(D) - \rho_{va}}{D}, \tag{14.20}$$

where $\rho_v(D)$ is the water vapor density in the soil at a depth D in the DSL, ρ_{va} is the atmospheric water vapor density near the surface, and K is the coefficient of diffusion in our DSL. K can be expressed by the molecular diffusivity of water vapor and soil air content to show the effective area for vertical diffusion, tortuosity, and so on. Kobayashi and Nagai (1995) reported the evaluation of evaporation of several days at the same desert station above-mentioned using a laboratory evaluated K as a function of water content and temperature. The water also brings soil solute

materials and releases them during evaporation. Thus, evaporation in arid areas is important in considering salinization. Experimental studies in laboratories were done using sample sand in Shimojima and Tamagawa (2001) and those in other studies where the DSL condition is considered.

As shown briefly, even in the simple conditions of sand deserts, evaporation still involves several processes, including water vapor diffusion in unsaturated layers, especially in the DSL. The water vapor gradient in the DSL connected the groundwater condition at the bottom of the DSL to the atmospheric humidity to determine the evaporation rate E. E affects the water amount in sand and thus can change the DSL depth. The processes in the DSL determine the evaporation amount in arid areas. The amount of evaporation is not large, but it determines soil water conditions. For the heat budget, λE in (14.1) disappears, and cooling by evaporation occurs in the evaporation level around the bottom of the DSL. This thin layer cooling may not be correctly measured with the thermometer in the sand. The amount of total cooling due to evaporation is still λE, and (14.1) can be applied to analyzing the observed data.

The most numerical simulation model on land surface processes assumes that the water content of the top layer of soil determines the evaporation rate. This is a little bit of rough treatment for evaporation in arid areas, although the computed water content is roughly adaptable, and the evaporation amount is small in arid areas. Several models were developed to include these processes. For example, Katata et al. (2007) included water and water vapor processes in soil and compared their results with commonly used land surface models in arid conditions. The developed model could perform well in showing the behavior of nightly adsorbed water in the DSL and its effects on surface temperature variations. Scanlon et al. (2003) also applied for the Philip and de Vries type model for the long-term simulation of water and chloride simulation.

As very shortly stated above, processes in soil layers are very important in arid areas. This is an actual limiting evaporation stage in arid areas. Measurements in soil seem to be still difficult in arid areas, for example, because sand-surface-level changes due to the movement of sand by wind and the high density of solute materials affect the electromagnetic characteristics of the water used in the water content measurement.

14.4 Conclusion

Topics relating to evaporation in arid areas were introduced. First, meteorological processes related to evaporation, such as the surface heat budget and turbulent transfer of heat and water vapor with Monin–Obukhov similarity theory, were explained with care for arid conditions. The results obtained from an old HEIFE project were used to explain the processes applied to evaluate evaporation. We explained the eddy covariance observation for a measured evaporation rate directly with turbulence observation as well as the heat budget relationship and the Monin–

Obukhov similarity in considering the observed results to connect the direct observed turbulent flux with the mean atmospheric variables. We suggest that the readers refer to the suggested readings for a more comprehensive understanding of micrometeorology. Soil physics was also briefly introduced, focusing on the DSL. The processes in the DSL microphysically determined the evaporation rate. Atmospheric processes only transferred water vapor and gave boundary conditions to the DSL from a soil process viewpoint. We have to recognize that the soil and the atmosphere are strongly connected to each other and must be considered as one system.

This kind of observational work has been done over many places in the world. The readers may read the results in other climate regions. Even operationally, worldwide meteorological observation networks and numerical weather or climate simulations are now available. However, it should be noted that observation networks and numerical models are neither perfect nor dense enough. Thus, observational studies are necessary for understanding phenomena in detail. These are also useful as ground truth data for simulations and remote sensing to validate and improve results.

References

de Vries DA (1958) Simultaneous transfer of heat and moisture in porous media. Trans Am GeophysUnion 39:909–916

Fleagle RG, Businger JA (1980) An introduction to atmospheric physics, 2nd edn. Academic press Inc., 432

Foken T (2008) Micrometeorology. Springer 306

Hillel D (2004) Introduction to environmental soil physics. Elsevier Science, p 494

Kader BA, Yaglom AM (1990) Mean fields and fluctuation moments in unstably stratified boundary layers. J Fluid Mech 212:637–662

Kaimal JC, Finnigan JJ (1994) Atmospheric boundary layer flows. Oxford University Press, p 289

Katata G, Nagai H, Ueda H, Agam N, Berliner PR (2007) Development of a land surface model including evaporation and adsorption processes in the soil for the land–air exchange in arid regions. J Hydrometeorol 8(6):1307–1324

Kobayashi I, Nagai H (1995) Measuring the evaporation from a sand surface at HEIFE desert station by the dry surface layer (DSL) method. J Meteorol Soc 73:937–945

Leuning R (2007) The correct form of the Webb, Pearman and Leuning equation for eddy fluxes of trace gases in steady and non-steady state, horizontally homogeneous flows. Boundary-Layer Meteorol 123:263–267

Mitsuta Y (2005) Sino-Japanese joint research project HEIFE: general view and results. J Nat Disaster Sci 22(1):45–51

Mitsuta Y, Tamagawa I, Sahashi K, Wang J (1995) Estimation of annual evaporation from the linze desert during HEIFE. J Meteor Soc Japan 73:967–974

Monji N (1973) Budgets of turbulent energy and temperature variance in transition zone from forced to free convection. J Meteor Soc Japan 51:133–145

Philip JR, de Vries DA (1957) Moisture movement in porous materials under temperature gradients. Eos Trans AGU 38:222–232

Scanlon BR, Keese K, Reedy RC, Simunek J, Andraski BJ (2003) Variations in flow and transport in thick desert vadose zones in response to paleoclimatic forcing (0–90 kyr): field measurements, modeling, and uncertainties. Water Resour Res 39:1179

Shimojima E, Tamagawa I (2001) Salinity on water and solute movement in a sand column induced by evaporation. J Japan Soc Hydrol Water Res 14(2):121–130

Stull RB (1988) An introduction to boundary layer meteorology. Springer 688

Tamagawa I (1996) Turbulent characteristics and bulk transfer coefficients over the desert in the HEIFE area. Boundary-Layer Meteorol 77:1–20. https://doi.org/10.1007/BF00121856

United Nations Environment Programme (2006) Global desert outlook, Edited by Exequiel Ezcurra, Division of Early Warning and Assessment (DEWA), United Nations Environment Programme, P.O. Box 30552, Nairobi 00100, Kenya, ISBN: 92–807–2722-2, UNEP Job No. DEW/0839/NA, 148

Webb EK, Pearman GI, Leuning R (1980) Correction of flux measurements for density effects due to heat and water vapour transfer. Quart J Roy Meteorol Soc 106:85–100

Wang J, Mitsuta Y (1991) Turbulence structure and transfer characteristics in the surface layer of the HEIFE Gobi area. J Meteor Soc Japan 51:587–593